ELSEVIER

NeuroImage

www.elsevier.com/locate/ynimg
NeuroImage xx (2006) xxx–xxx

A spatially unbiased atlas template of the human cerebellum

Jörn Diedrichsen*

Laboratory for Computational Motor Control, Department for Biomedical Engineering, Johns Hopkins University School of Medicine, Baltimore, MD 21205, USA

Received 28 February 2006; revised 16 May 2006; accepted 23 May 2006

This article presents a new high-resolution atlas template of the human, cerebellum and brainstem, based on the anatomy of 20 young healthy individuals. The atlas is spatially unbiased, i.e., the location of each structure is equal to the expected location of that structure across individuals in MNI space, a result that is cross-validated with an independent sample of 16 individuals. At the same time, the new template preserves the anatomical detail of cerebellar structures through a nonlinear atlas generation algorithm. In comparison to current whole-brain templates, it allows for an improved voxel-by-voxel normalization for functional MRI and lesion analysis. Alignment to the template requires that the cerebellum and brainstem are isolated from the surrounding tissue, a process for which an automated algorithm has been developed. Compared to normalization to the MNI whole-brain template, the new method strongly improves the alignment of individual fissures, reducing their spatial spread by 60%, and improves the overlap of the deep cerebellar nuclei. Applied to functional MRI data, the new normalization technique leads to a 5–15% increase in peak *t* values and in the activated volume in the cerebellar cortex for movement vs. rest contrasts. This indicates that the new template significantly improves the overlap of functionally equivalent cerebellar regions across individuals. The template and software are freely available as an SPM-toolbox, which also allows users to relate the new template to the annotated volumetric (Schmahmann, J.D., Doyon, J., Toga, A., Petrides, M., Evans, A. (2000). MRI atlas of the human cerebellum. San Diego: Academic Press) and surface-based (Van Essen, D.C. (2002a) Surface-based atlases of cerebellar cortex in the human, macaque, and mouse. *Ann. N. Y. Acad. Sci.* 978:468–479.) atlas of one individual, the "colin27"-brain.

Keywords: Normalisation; Cerebellum; Atlas; functional MRI

Introduction

While the simple and homogenous cerebellar micro-circuitry suggests a uniform computational function of this structure, a unified theory of cerebellar function remains elusive. A number of hypotheses have been proposed, including the coordination of movement across different joints (Thach et al., 1992), timing (Ivry et al., 2002), internal models (Wolpert et al., 1998), or the cerebellum as a fast learning machine (Albus, 1971). With the advent of neuroimaging, it has also become apparent that parts of the cerebellum are involved in sensory (Gao et al., 1996), and cognitive processes (Courchesne and Allen, 1997).

Underlying this apparent functional heterogeneity is the fact that, while the cytoarchitecture of the cerebellum is homogenous, inputs and outputs are not: the cerebellum receives afferent fibers through the pons from nearly every cortical area (Schmahmann, 1996). These fibers appear to terminate in specialized regions of the cerebellar cortex and form closed loops with their respective cortical targets (Middleton and Strick, 1997; Kelly and Strick, 2003). While distinct functional areas in the cerebral cortex are of the size of multiple cm^2, distinct subregions of the cerebellum may occur on a much smaller scale.

In applying functional magnetic resonance imaging (fMRI) to the cerebellum, the small scale of functionally distinct regions constitutes a major challenge. How does one combine anatomical and functional data across participants, given the considerable anatomical variability between individuals, and the rather small size of functional subunits? One possibility is to parcellate each cerebellum based on the individual anatomy into a set specific regions, e.g., individual lobules (Pierson et al., 2002; Makris et al., 2003, 2005). For functional analysis one would then average the BOLD signal within each region and subsequently average each region across individuals (Desmond et al., 1997, 1998). Although such region-of-interest based approaches have been quite successful in single cases, they are not widely used because they are very labor intensive. More importantly, they limit analysis to a set of distinct set of subregions and do not allow for a more fine-grained voxel-based analysis.

Voxel-based approaches, in contrast, attempt a continuous mapping between the individual anatomy and a specific template (Woods et al., 1998b; Ashburner and Friston, 1999). In such approaches, the template image, $g(x)$, is matched to an individual image, $f(y)$, using the deformation map, $y_i = x_i + v(x_i)$, where x and y constitute locations in template and individual image, respectively. The deformation can be found by minimizing the

* School of Psychology, Adeilad Brigantia, University of Wales Bangor, Gwynedd LL572AS, UK. Fax: +410 614 9890.
E-mail address: j.diedrichsen@bangor.ac.uk.
Available online on ScienceDirect (www.sciencedirect.com).

1053-8119/$ - see front matter © 2006 Elsevier Inc. All rights reserved.
doi:10.1016/j.neuroimage.2006.05.056

cost function J, the squared voxel-by-voxel difference between the template g and thedeformed source image f:

$$J = \sum_i (f(x_i + v(x_i)) - g(x_i))^2 \quad (1)$$

In the simplest case, the deformation map **v** can be conceptualized as a 12-parameter affine transform (Woods et al., 1998b), $y_i = Ax_i + c$, allowing for translation, rotation, scaling and shearing of the template space to map onto the individual's brain. For the cerebellum an affine alignment has been used by Grodd et al. (2001), only allowing for translation and scaling. This approach relied on a set of manually defined landmarks. Another popular approach, also utilized in this paper, uses cosine basis functions (Ashburner and Friston, 1999) to allow for nonlinear deformations (see Methods).

Currently, the most widely used template for voxel-based analysis is a template from the Montreal Neurological Institute (MNI), accepted as a standard by the International Consortium for Brain Mapping (ICBM). This template, the ICBM152, was generated by averaging 152 anatomical scans after correcting for overall brain size and orientation (Evans et al., 1993). As a result, the template provides very little anatomical detail. This, as we show below, leads to poor alignment of cerebellar structures, limiting the usefulness of a voxel-based approach for infra-tentorial structures.

To overcome these limitations, we aimed at developing an atlas template of the cerebellum and brainstem that represents the average geometry of a sample of individuals, while still providing enough anatomical detail to ensure that individual lobules within the cerebellum can be aligned. Such a template should therefore improve the overlap of cerebellar structures, while retaining the advantages of a voxel-based approach (Woods et al., 1998b; Ashburner and Friston, 1999).

One possible solution for a template would have been to use the cerebellum of a particular individual, for example colin27, a young individual who was scanned 27 times at the Montreal Neurological Institute. The cerebellar anatomy of this individual has been carefully documented (Schmahmann et al., 2000), and a flattened representation of this cerebellum has been created (Van Essen, 2002b). However, using a single individual's anatomy as a template, as was done by Talairach and Tournoux (1988), has an important drawback: every individual shows some anatomical idiosyncrasies that are not representative of the population. When normalizing a sample of individual brains to this space, systematic deformations would arise, which could affect both functional and anatomical studies of the cerebellum.

Therefore, our goal was to make a spatially unbiased template (for a similar argument, see Woods et al., 1998a). With this we mean that the location of any particular structure i in the new atlas template should be equal to the average, or expected, location of that structure across all individuals n:

$$E(y_i^{(n)}) = z_i \ \forall i \quad (2)$$

Spatial bias can only be defined in respect to a common reference frame in which locations across individuals can be compared. As a commonly accepted reference frame, we chose here the ICBM152 template. Therefore, the new cerebellar template was generated using a group of 20 participants that had undergone an affine alignment to the ICBM152 whole-brain template. To limit the template and the normalization to the cerebellum and brainstem, we developed an algorithm that isolates the cerebellum and brainstem from the surrounding tissue. This ensures that the boundaries of the cerebellum are properly aligned across individuals. After isolation, all cerebella underwent a nonlinear normalization to a single individual cerebellum, and were averaged. This average image was then deformed using the inverse average deformation, creating a new Spatially Unbiased Infratentorial (SUIT) template. As a result, the coordinates of a structure in the new template are equal to the average coordinates of that structures across individuals (Eq. (2)). At the same time, by using the isolation algorithm and a high-resolution nonlinear deformation, the new template preserves much more anatomical detail than the whole-brain template.

We show in an independent cross-validation sample of 16 participants that the new atlas template leads to a significantly improvement in overlap of individual cerebellar fissures and of the deep cerebellar nuclei. We also show that the template significantly improves the analysis of functional data, making the new template a useful tool for functional and lesion analyses of the human cerebellum.

Methods

Participants

The atlas is based on anatomical data from 20 neurologically healthy subjects (11 females and 9 males). Their ages ranged from 22 to 45 years, the mean age was 27.25 years. The atlas group was comprised of 13 participants from Exp 1 in Diedrichsen et al. (2005) and 7 new participants. For cross-validation we used the 16 participants (6 females and 10 males, ages 18–29 years, mean age 23. 8 years) that had participated in Exp 2 of the same study. The Johns Hopkins School of Medicine Internal Review Board approved the study procedures.

Data acquisition

Data were acquired on a 3T Philips Intera system (Philips Medical Systems, Best, Netherlands). T1-weighted structural images with a field of view of 256×256×150 mm were acquired with 1×1×1 mm resolution using a MPRAGE sequence. TR was 8.25 ms and scan duration 575 s. Six receiver coils were used for Sensitivity-Encoded MRI (Pruessmann et al., 1999), however, for better signal-to-noise ratio k-space was fully sampled, i.e., the SENSE factor was set to 1.

The functional protocols for Exp 1 and 2 have been described previously (Diedrichsen et al., 2005). The whole brain was covered in 37 axial slices (3 mm thickness, 0.5 mm gap, TR=2 s, SENSE factor=2), each of which was acquired as an 80×80 matrix (FOV was 24.0×24.0 cm), with a resultant voxel size of 3×3×3.5 mm.

Isolation algorithm

To ensure that only infra-tentorial structures are aligned to the atlas template, the normalization procedure requires that the cerebellum and brainstem to be isolated from the surrounding tissue. This is necessary because cortical and cerebellar gray matter has similar brightness values, and the cost function (Eq. (1)) would otherwise fail to align the boundary between the visual cortex and the anterior cerebellum. The isolation procedure is based on a stepwise Bayesian integration of three pieces of information (Fig. 1) to determine the posterior probability of each voxel i belonging

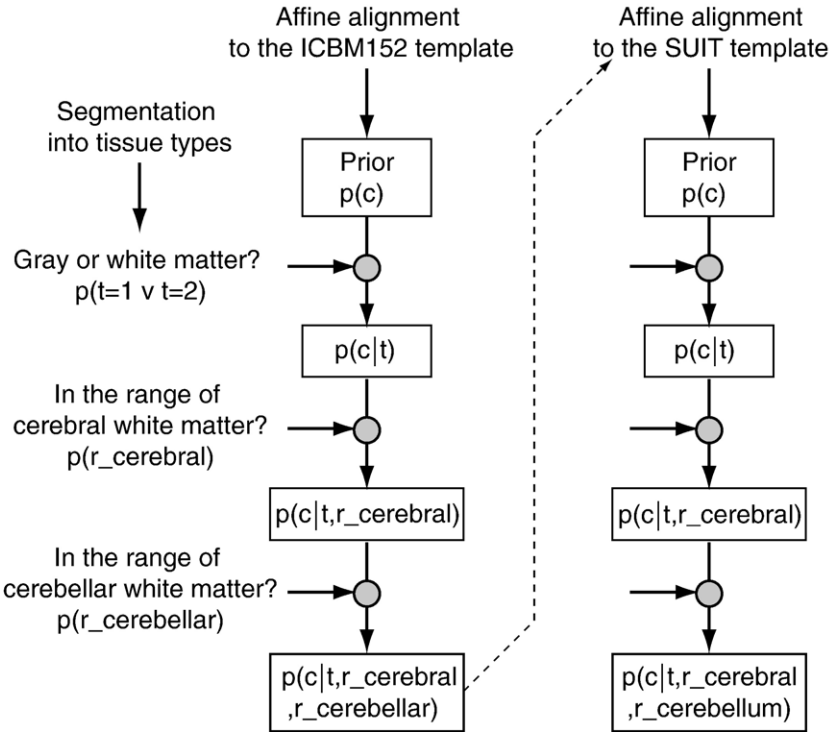

Fig. 1. Algorithm for isolation of the cerebellum and brainstem from the surrounding tissue. The algorithm starts with a prior probability defined in the MNI space and uses Bayes rule (Eq. (3), gray circles) to integrate new information on each step. The posterior probability from the first iteration (left column) is then used as a mask to normalize to the SUIT template, repeating the algorithm with a more accurate prior (right column).

to the cerebellum or brainstem (indicated by the Boolean variable $c_i=1$). The three pieces of information are:

1. The prior probability of any voxel to be part of the cerebellum or brainstem, $p(c_i)$. To generate this prior probability map we manually generated classification maps ($c_i=1$ for cerebellum or brainstem, 0 for other) for the 20 individuals, aligned them to the ICBM 152 template, averaged them, and finally smoothed them with a 3-mm Gaussian kernel. This prior probability map is projected into the native space of the subject by finding the affine whole-brain alignment of that subject to the ICBM 152 template.
2. The tissue type t_i of the voxel i. An existing probabilistic segmentation algorithm (Ashburner and Friston, 2005) is used to calculate the probability of a voxel to be gray matter, $p(t_i=1)$, white matter, $p(t_i=2)$, or CSF, $p(t_i=3)$. The algorithm combines the voxel intensities after nonuniformity corrections with the prior probabilities in the reference frame of ICBM template. The prior probability maps are derived from whole-brain segmentation and show very low probabilities of gray and white matter for inferior parts of the cerebellum, most likely due to image inhomogeneities in the original sample. This causes the inferior regions of the cerebellum to be classified as nonbrain voxels. We therefore modified the prior probabilities in the inferior aspects of the cerebellum based on the 20 individuals whose cerebella were isolated and segmented by hand.
3. The spatial proximity of gray matter voxels to either cerebral or cerebellar white matter. White matter voxels can be easily classified as belonging to the cerebellum or the cerebrum based on their connectivity with other white matter voxels and the relative spatial location of these white matter clusters. Within each slice, the algorithms classifies clusters, i.e. connected voxels of white matter, as belonging to the cerebrum or the cerebellum by averaging the prior probability $p(c_i)$ over all voxels within a cluster.

If the probability exceeds 0.5, the cluster is classified as cerebellar white matter, if it was lower than 0.5, as cerebral white matter. After white matter has been divided in this way, we use the fact that neo-cortical gray matter is typically found in a range of 3.5 mm of the cerebral white matter and the cerebellar gray matter in general in a range of 2.5 mm of the cerebellar white matter. To approximate the probability that a voxel is in the range of at least one cerebral white matter voxel, $p(r_i^{cerebral})$, we convolve the probability map of being a cerebral white matter voxel with a 3-d boxcar function with a width of 7 mm. A similar procedure is used to estimate the probability that each voxel is in the range of at least one cerebellar white matter voxel, $p(r_i^{cerebral})$.

These pieces of information are then integrated using a Bayesian approach (Fig. 1). Each integration step uses a prior probability, $p(c)$, and the probability that statement x is true, given evidence E from the raw image, $p(x|E)$. The state x can be the fact that a voxel is of a particular tissue type, or that the voxel is in the range of cerebellar/cerebral white matter. The application of Bayes rule also requires the conditional probabilities of x if the voxel belongs to the cerebellum or brainstem, $p(x|c)$, and if it does not $p(x|\neg c)$. Generally, the posterior probability of $\boldsymbol{c}$ given the evidence from the image can be calculated as:

$$p(c|E) = p(x|E)\frac{p(x|c)p(c)}{p(x|c)p(c)+p(x|\neg c)p(\neg c)} + p(\neg x|E)\frac{p(\neg x|c)p(c)}{p(\neg x|c)p(c)+p(\neg x|\neg c)p(\neg c)} \quad (3)$$

For the tissue information, x represents the event that the voxel is either gray or white matter. Because the cerebellum consists only of gray or white matter, the probability $p(\neg x|c)$ is zero and the second term vanishes. All other conditional probabilities were calculated from the manually defined cerebellar classification maps used for atlas generation.

After tissue information, spatial range information is integrated accordingly. The prior probability at this step is set to the posterior probability from the previous step. Range information is integrated in two separate steps, one for the cerebral, one for the cerebellar white matter. All these computations are performed in a $14 \times 9.4 \times 7.4$ cm bounding box around the cerebellum and brainstem.

The isolation procedure relies heavily on the initial prior probability, which is based on finding an alignment between the individual and the reference frame in which the prior is defined. To improve the accuracy of this prior information, the algorithm runs through the steps described above twice (Fig. 1). During the first iteration, a prior in the space of the ICBM152 template is used and sampled into the space of the individual using an alignment. The preliminary segmentation obtained by the first iteration serves as a weight map for an affine alignment to the new infra-tentorial template, such that only the tissue that has been identified as belonging to the cerebellum or brainstem influences the alignment. During the second iteration, a new prior defined in the SUIT template space, which was obtained by averaging the classification maps of the atlas group after affine alignment to the infra-tentorial template. Because of the improved anatomical alignment, this prior is much more clearly defined than the prior used in the first iteration, therefore improving the classification results.

To obtain smooth edges on segmentation, the final probability map was smoothed with a Gaussian kernel of 3-mm FWHM. The resulting probability maps were visually inspected, and, if necessary, hand corrected (see Results). For hand correction, the probability map was thresholded at $p = 0.5$ and manipulated using CARET (Van Essen et al., 2001). To reapproximate a probability map, this binary hand correction was then smoothed with a 3-mm kernel.

Normalization procedures

The normalization of an individuals to a template relies on techniques developed by Ashburner et al. (1999), implemented in the SPM2 package (Friston et al., 1999) and the deformations toolbox. The deformations are parameterized as an affine transformation (A, c) including shear, scaling, rotation and translation, and a nonlinear deformation vector field $v(x)$. This vector field is approximated using a set of $i \times j \times k$ cosine basis function for deformations in each of the 3 directions d:$b_{ijk}^{(d)}(x)$.

$$v^{(d)}(x) = \sum_{i=1}^{I} \sum_{j=1}^{J} \sum_{k=1}^{K} t_{ijk}^{(d)} b_{ijk}^{(d)}(x) \tag{4}$$

$$y = A(x + v(x)) + c$$

The basis functions are generated by taking the Cartesian product of a set of three one-dimensional cosine basis functions. A Newton–Raphson algorithm is used to find the best estimate for the coefficients of the nonlinear basis functions.

Standard normalization in SPM2 uses the ICBM152 template in a bounding box of $18.2 \times 21.8 \times 18.2$ cm, and basis functions up to a cutoff frequency of 2.5 cm, yielding a total of 441 basis functions for each dimension (7 in x-, 9 in y-, and 7 in z-direction). Because the template lacks fine anatomical detail, the source image is smoothed, as standard in SPM, with an 8-mm Gaussian kernel before normalization.

For cerebellar normalization we use a $14.1 \times 9.5 \times 8.7$ cm template and basis function down to a cutoff frequency of 1 cm, yielding 1120 basis function for each direction (14 in x-, 10 in y-, and 8 in z-direction). Before alignment to the cerebellar template the individual images are multiplied with the probability map obtained by the segmentation algorithm, retaining only infra-tentorial structures. Because the cutoffs for the brainstem above and below the pons are arbitrary, these boundaries are excluded from the normalization by multiplying the cost function (Eq. (1)) with a weighting image $w(x)$. In this image, the values of brainstem structures above the pons and below the medulla oblongata are set to zero. The location of the brainstem cutoff, therefore, does not influence the normalization procedure. Given the higher anatomical detail in the template, the source image is smoothed with a 2-mm Gaussian kernel prior to normalization.

Generating an unbiased infra-tentorial template

The process of generating a spatially unbiased atlas template for the new cerebellar template is depicted in Fig. 2. First, we found a 12-parameter affine transformation (A_i) between each individual anatomical image and the ICBM152 template by minimizing the voxel-by-voxel cost-function (Eq. (1)), normalizing for brain size, rotation, offset and shear. The cerebellum and brainstem were then isolated for each individual using the described method, and, if necessary, manually corrected. The original anatomical image was multiplied with the resulting probability map, retaining only cerebellum and brainstem. These images were then normalized to the colin27 cerebellum using a nonlinear deformation field consisting of cosine basis functions. For every location x_i in the colin27 cerebellum, we found a deformation vector $v_i^{(n)}$ that mapped the colin27 space into the space of the nth subject: $y_i^{(n)} = x_i + v_i^{(n)}$. These deformations were then averaged $\overline{v}_i = 1/20 \sum_{n=1}^{20} v_i^{(n)}$ and a new template space was defined as $z_i = x_i + \overline{v}_i$. As a result this new space was spatially unbiased with respect to the original group of individuals, i.e., the expected deformation vector between y_i and z_i is zero. To arrive at the new template image, we resampled each individual into the new space defined by z, using trilinear interpolation and averaged the resulting images. These computations were conducted numerically using the deformation toolbox. Whenever possible, deformations were combined and resampling was performed directly from the original images.

This process was repeated 2 times, each time replacing the target image with the new cerebellar atlas template. Although the geometry of the template changed minimally after the first cycle, we found that this process improved the gray/white matter contrast of the new cerebellar template. It is important to note that we would have arrived at an identical atlas space if we had used the cerebellum of any of our participants as the first template, as the definition of spatial bias (Eq. (2)) does not depend on a particular choice of the initial template x. By using the colin27 brain, however, we were able to calculate deformation maps between the colin27 cerebellum and the new atlas space. Therefore, the existing MRI atlas of the cerebellum (Schmahmann et al., 2000) and the cerebellar flatmap (Van Essen, 2002a) can be easily utilized within this new reference frame.

We repeated the above process on the same 20 individuals a second time using a nonlinear warp to the ICBM152 template

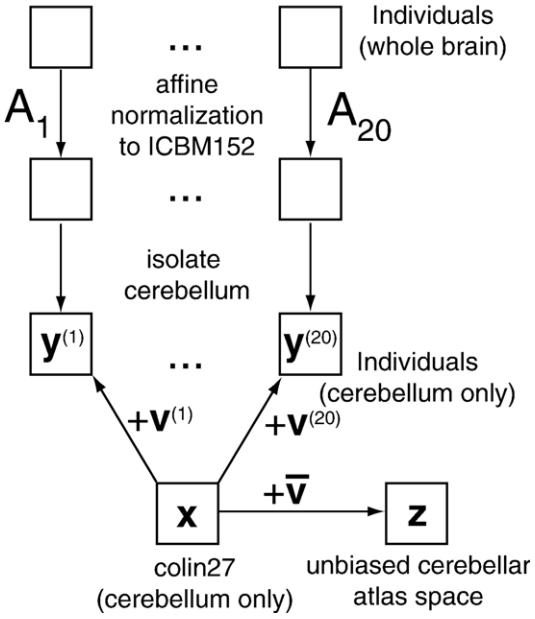

Fig. 2. Generation of a spatially unbiased infra-tentorial atlas template. Individual anatomical scans (T1, 1 mm MPRAGE) were aligned to the ICBM152 template using affine alignment (A). The cerebellum and brainstem were then isolated from the surrounding tissue. A nonlinear deformation ($v^{(n)}$) was found between the isolated cerebellum and brainstem of one individual, colin27, and each of the current participants. The individual images were averaged in the space defined by colin27. The nonlinear deformation fields were averaged ($\bar{v}$), and this deformation was applied to the averaged image. The process was repeated two times, each time replacing the colin27 cerebellum with the new template.

(using the SPM2 default normalization) instead of the affine alignment as the first step. Surprisingly, we found systematic differences between the affine and nonlinear whole-brain normalization (see results). For this reason, we also generated a spatially unbiased cerebellar template for the nonlinear ICBM152 normalization (SUIT*).

Measures of anatomical overlap

To quantify the degree of anatomical overlap, we used three criteria: the voxel-by-voxel correlation between images, the spatial consistency of two selected fissures, and the spatial overlap of the deep cerebellar nuclei. For the first measure, we computed all possible pair-wise correlations between individual anatomical images after normalization with one of the four methods (Affine or nonlinear normalization to the ICBM152 template, SUIT, or SUIT*). The correlations were computed voxel-by-voxel within a mask spanning the cerebellum plus a 1-cm rim around it. This method allows for the evaluation of both the internal overlap and the correspondence of the edges. These computations were performed for the 20 individuals in the atlas group and for the 16 individuals in the cross-validation group.

To measure the spatial spread of anatomically equivalent structures after alignment, we marked two fissures on each of the 16 cross-validation participants. We chose a major fissure, the primary fissure, which separates lobules V and VI, and a minor fissure, the intrabiventer fissure, which separates lobules VIIIa and VIIIb. The fissures were drawn as surfaces in the 3d-volume (Schmahmann et al., 2000), defined by vertices at a distance of ca. 3 mm from another. The surfaces were then subsampled to an inter-vertex distance of 1 mm and deformed using the affine or nonlinear normalization to the ICBM152, the SUIT, or SUIT* template. We then evaluated the alignment by computing, for each possible pair of participants, the average distance between corresponding surfaces. For each point on the source surface we found the minimal distance to a point on the target surface. These values were then averaged across all points of the source surface. For each possible pair this computation was performed in both directions, yielding similar, but due to the finite sampling of the surface, not identical values.

To determine the overlap of the deep cerebellar nuclei after normalization, we outlined these nuclei as regions of interest (ROI) on the mean functional image of each individual in the cross-validation group. Due to their high iron content, the nuclei are visible as hypo-intensities on these T2*-weighted images (Dimitrova et al., 2005). Although the low resolution of the functional images only provided a rough estimate of the location of the deep cerebellar nuclei, the main emphasis was a comparison of the two normalization methods in terms of the degree of spatial overlap.

Functional analysis

To measure the influence of the new atlas in the analysis of functional data, we reanalyzed the data from a previously published study (Diedrichsen et al., 2005). All participants from Exp 1 ($N=13$) were part of the atlas group. To cross-validate the results, we reanalyzed the functional data from Exp 2 ($N=16$). Both experiments employed a blocked paradigm, in which blocks of ten point-to-point arm movements (20 s) alternated with blocks of 16 s rest. Exp 1 had three movement conditions (unperturbed, visual rotation and target jump) and two eye movement control conditions, while Exp 2 had only three movement conditions (unperturbed, visual rotation and force field).

A first-level general-linear model (GLM) was performed on the motion corrected functional data, excluding artifacts using a weighted-least squares method (Diedrichsen and Shadmehr, 2005). Percent signal change images were then computed for each condition. These images were then aligned to the high-resolution anatomical image of each participant. We applied two nonlinear deformations to the functional data. One was derived from the nonlinear normalization to the ICBM152 whole-brain template, using the default parameters in SPM2, the other was derived from normalization to the SUIT* template. All functional images were resampled at $2\times2\times2$ mm and smoothed with a 6-mm Gaussian kernel. For the cerebellar template, we masked the functional data before smoothing with the cerebellar segmentation to prevent activation of the visual cortex from bleeding into the anterior cerebellar lobe.

Results

Isolation of cerebellar and brainstem

Isolation of the cerebellum and brainstem from surrounding tissue took approximately 4 min per individual on a standard PC-laptop machine. A successful example of resulting probability maps is shown in Fig. 3A. The outline of the cerebellum is clearly defined and the map could be used without manual correction for the subsequent normalization steps. In the majority of the individuals, however, it was necessary to manually correct the segmentation because of frequently occurring defects. In many of

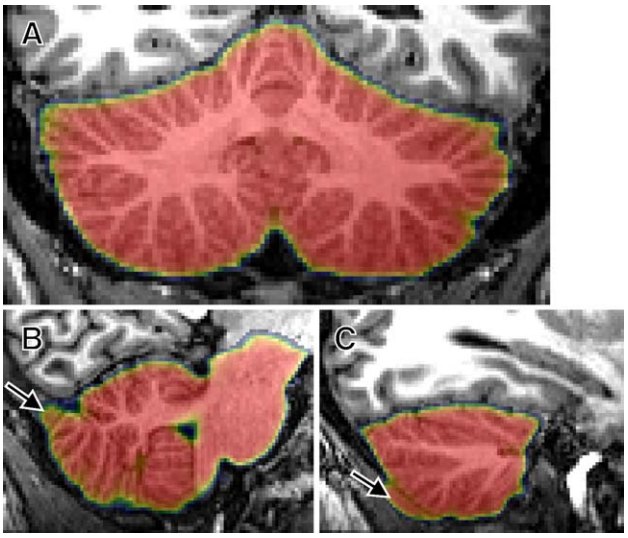

Fig. 3. Isolation of cerebellum and brainstem. The resulting posterior probability (thresholded at 0.5) is overlayed on a T1 anatomical image. Probabilities range from 1 (red) over 0.75 (yellow) to 0.5 (blue). A successful segmentation (A) and two commonly occurring errors are shown. The transverse sinus is often marked as part of the cerebellum (B). More rarely, the segmentation sometimes also extends into the bone marrow (C).

the individuals, parts of the transverse sinus or the cerebellar tentorium, the hard membrane that separates the cerebellum from cortex, was marked as part of the cerebellum (Fig. 3B, arrow). Less frequently, but more damaging to subsequent normalization, part of the bone marrow was sometimes mistaken for cerebellar gray matter (Fig. 3C, arrow). If necessary, manual correction of the cerebellum took 5–10 min per individual.

Generation of template

We generated the new spatially unbiased infra-tentorial (SUIT) template, following the nonlinear atlas generation algorithm described in the methods (Fig. 2). We deformed each of the individual isolated cerebella into the new space defined by the average geometry and averaged the anatomical images. The resulting image has a coordinate system that is compatible with that defined by the ICBM152 template (Fig. 4). Compared to the whole-brain alignment (Fig. 5A), the new template preserves the anatomy of the cerebellum with higher spatial detail. All individual lobules are clearly visible.

It should be noted however, that while the new atlas template is unbiased in respect to the ICBM152 template, it suffers from the same bias as the ICBM152 template itself. Specifically, during the affine alignment to the ICBM152 template our atlas brains were magnified on average by 8% in the *x*-, 6% in the *y*-, and 19% in the *z*-direction, a bias has been reported previously (page 347, Ashburner et al., 1997). Therefore, the new cerebellar template is slightly larger than the average cerebellum (Grodd et al., 2001).

Differences between whole-brain normalization methods

Instead of the affine 12-parameter alignment to the ICBM152 whole-brain template, we also used a 1323-parameter nonlinear normalization, using the default values in SPM2. Surprisingly, these two methods led to slightly divergent results. For example, cerebellum after nonlinear normalization (Fig. 5B) was more elongated in *z*-direction than after affine normalization (Fig. 5A).

To test whether nonlinear alignment led to a systematic deformation compared to affine alignment, we calculated the deformation field between the two methods. We tested the null

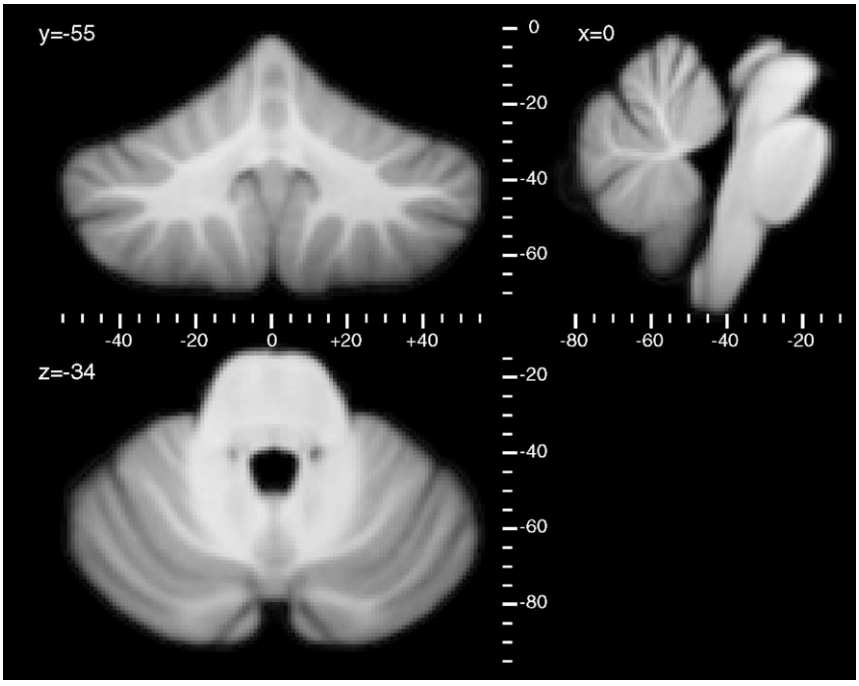

Fig. 4. Coronal, horizontal and sagittal view of the Spatially Unbiased Infra-tentorial (SUIT) template. The coordinate system is defined by the ICBM152 template. Each structure is at the same coordinate as it would be on average after affine alignment to the generally accepted MNI reference frame. The template image is based on the average anatomical image of 20 individuals.

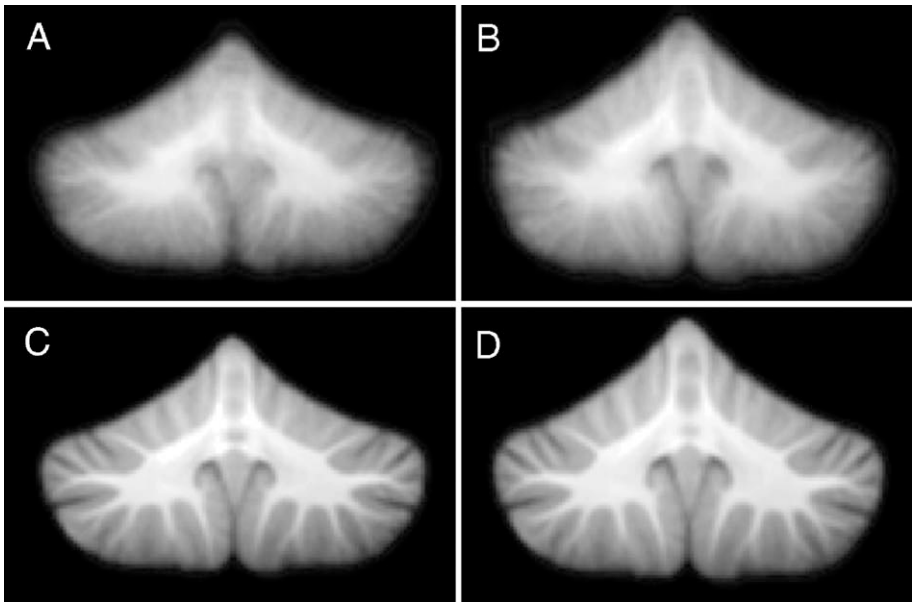

Fig. 5. Average anatomical image of the cerebellum of 20 participants after (A) affine whole-brain alignment to the ICBM152 template, (B) nonlinear normalization to the ICBM 152 using cosine basis functions with 2.5 cm cutoff frequency, (C) nonlinear normalization (1 cm cutoff frequency) to the unbiased infra-tentorial template with respect to the affine registration (SUIT), (D) nonlinear normalization to the unbiased infra-tentorial template with respect to a nonlinear normalization with cosine basis functions (SUIT*).

hypothesis that the average deformation vector at each point was zero, using the Hotellings T^2 statistic:

$$T^2 = n\bar{v}^T \Sigma^{-1} \bar{v} \quad (5)$$

in which n is the number of individuals, $\bar{v}$ is the mean vector at a voxel location, and Σ the variance–covariance matrix of the vectors. The statistic $F=(n-p)/(n-1)pT^2$ has approximately F-distribution with p and $n-p$ degrees-of-freedom, where p is the dimensionality of the vector (in our case 3).

The most significant deformation, $F(3,17)=94.2$, $p<0.001$, was found in the middle of the ICBM152 atlas template, at the coordinate (0, −52, 11). Here the average shift in the z-direction was 5. 5 mm upward compared to the affine normalization, highly systematic across individuals. The lower boundary of the cerebellum showed a downward shift of 1. 5 mm, leading to the elongation that is visible in the comparison of Figs. 5A and B.

The reason for this systematic deformation is not entirely clear. However, the same result was obtained using SPM5, as well as the cross-validation sample. It is possible that contrast differences between template and individual images, or an inherent feature of the template or normalization method using cosine basis functions caused such systematic biases.

Given these results, we generated two separate atlas templates, a spatially unbiased infra-tentorial template in respect to the affine normalization to the ICBM152 template (SUIT), and a spatially unbiased infra-tentorial template in respect to the nonlinear normalization to the ICBM152 template (SUIT*). We strongly encourage use of former template, because it most closely represents the average size and geometry of the cerebellum. For analysis of fMRI data, however, nonlinear whole-brain normalization using cosine basis functions has become an accepted standard. Thus, for the purposes of this article, we will use the SUIT* template to compare results obtained with standard SPM2 normalization to normalization using an infra-tentorial template.

Size of spatial deformation and spatial bias

After aligning individuals to the new cerebellar templates (Fig. 4), we calculated the deformation vector between each point in the template **z** and the corresponding point in the individual image **y** (after normalization to the ICBM152 whole-brain template). The average and maximum length of the vectors $v(x)$ within the cerebellum (excluding the brainstem) provided a measure of the difference between the whole-brain and the cerebellar normalization method.

The average and maximum length of the deformation vectors within each participant provided a measure of how much the methods differed for an individual case. Across the 20 participants, the average length was 3–4 mm and the maximum length 9 mm. Similar results were obtained in the cross-validation group (Table 1A). Thus, for each individual participant, normalization to the cerebellar template substantially altered results compared to the whole-brain normalization.

The mean and maximum length of the average deformation vector (Table 1B) indicates how much the cerebellar normalization differed systematically from the whole-brain normalization. Because the new templates were designed to be spatially unbiased, the average deformation between whole-brain and cerebellar normalization should be zero (Eq. (2)). For the 20 atlas brains, the average length of the deformation vector was 0.3 mm with a maximum length of 1 mm, both for the SUIT and SUIT* templates. Although very small, the average deformation did not vanish completely. Fig. 6, which displays the remaining average deformation in x- and y-directions, hints at a possible reason. In the pons, for example, the average deformation from atlas to individual showed a rightward shift on the left side and a leftward shift on the right. The deformation vectors at the edges of the pons

Table 1
Mean and maximal size of the nonlinear deformation vectors within the cerebellum

	Affine vs. SUIT		Nonlinear vs. SUIT*	
	Atlas	Crossval	Atlas	Crossval
A. Size of deformation for individuals (mm)				
Mean	3.60	4.51	3.24	3.38
	(0.98)	(1.13)	(0.77)	(0.63)
Max	8.79	9.93	9.15	9.04
	(1.13)	(1.95)	(1.99)	(1.45)
B. Size of systematic deformation (mm)				
Mean	0.33	1.38	0.34	1.48
Max	1.01	3.07	1.48	3.65

Deformations are defined for each cerebellum between the affine alignment to the whole-brain ICBM152 template and the SUIT template (columns 1–2), as well as between the standard SPM2 nonlinear normalization to the ICBM152 template and the SUIT* template (columns 3–4). Results are provided for the individuals defining the atlas ($N=20$) and for a set of cross-validation individuals ($N=16$). (A) The average and maximum length of the deformation vectors (SD in parenthesis) computed within each individual indicates how much the two normalization methods differed for a given case. (B) The average and maximum of the average deformation map captures the size of the systematic differences (biases) between the two methods.

were near zero. This deformation would shift voxels within the pons, where there was no brightness contrast, but would leave the outline untouched. Therefore, the mean anatomical image did not change when this deformation was applied to it. Similar remaining deformations were observed in the posterior end of the cerebellum, where folia run in the horizontal direction. Remaining deformations therefore can occur in places where the cost function (Eq. (1)) does not provide any constraints for deformations in that direction. It should be noted, however, that the remaining deformations were very small, below 1 mm in size.

To test whether the average deformation vector was significantly different from zero, i.e., whether there were significant spatial biases, we used Hotellings T^2 statistics (Eq. (7)). We thresholded the maps at $p<0.005$ and used Gaussian field theory (Worsley et al., 1996) to correct for multiple comparisons over the volume of the cerebellum (excluding the pons and brainstem). For either the SUIT or SUIT* templates, none of the remaining deformations within the cerebellum were significant. Thus, within the bounds of individual variability, our method for generating a representative spatial template for the 20 cerebella was successful.

To test whether these templates were also representative for a new set of participants, we used the set of 16 cross-validation participants. The average deformation vector for these participants had a length of about 1 mm, with the maximal length being approximately 3 mm (Table 1B). For the SUIT template none of these biases reached significance when correcting for multiple comparisons. Indeed, only a small cluster of 17 mm^3 exceeded the uncorrected threshold of $p<0.005$, an event that is highly likely given the number of voxels tested.

In contrast, the average deformation vector of the 16 cross-validation scans to the SUIT* template showed a significant deformation vector in a cluster in the left crus II, $F(3,13)=61.2$, $p=0.007$, corrected. This deformation vector moved voxels from the nonlinear whole-brain alignment 2.2 mm superior and 0.9 mm anterior to the SUIT* template. Because this deformation was not found for alignment to the SUIT template, we suspect that this discrepancy was induced by the systematic spatial biases in the nonlinear whole-brain normalization, as observed in the systematic differences between the affine and nonlinear normalization methods reported above.

In conclusion, we show that whereas the SUIT* template may be somewhat biased, the SUIT template represents the average anatomy of a sample of cerebella from young, healthy individuals in a spatially unbiased fashion.

Anatomical measures

Figs. 5C and D show the average anatomical image of the 20 participants after normalization to the new infra-tentorial templates. These images are practically identical to the templates themselves, which were generated using the same method. The anatomical overlap appears dramatically improved. Even on the average anatomical image, all lobules and major fissures are clearly visible. To evaluate the anatomical overlap quantitatively, we used three measures; the correlations between anatomical images, alignment of fissures and overlap of deep cerebellar nuclei.

Anatomical correlations

The average pair-wise correlation between images (and the interval spanning 95% of the data) can be seen in Table 2. As expected, the affine whole-brain normalization led to the poorest overlap, with an average correlation of 0.84. When using the whole-brain nonlinear normalization, these correlations increased slightly to 0.87. However, the ranges of pair-wise correlations were overlapping. Our methods led to a jump of the pair-wise correlations to 0.97, with even the lowest correlation being higher than the highest obtained with the old methods. To ensure that these results did not solely reflect the fact that the template images represent the average geometry of those specific individuals, we cross-validated the results with anatomical data from 16 independent participants (Exp 2, Diedrichsen et al., 2005). The resulting anatomical correlations were in the same range as the results obtained with the 20 atlas brains (Table 2), showing the general applicability of the new method.

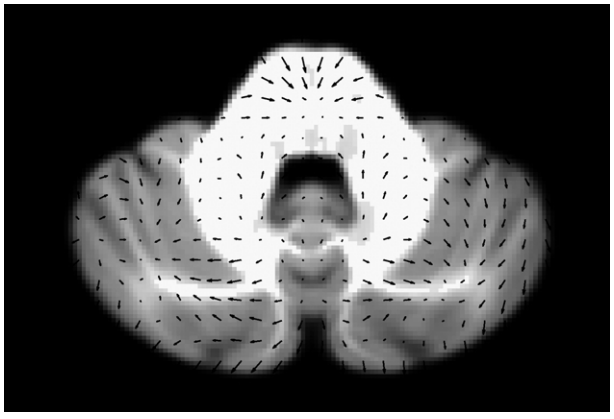

Fig. 6. Remaining spatial deformation in x- and y-directions after two iterations of the atlas generation procedure. Vectors indicate residual average deformation from individuals to atlas, magnified by factor 5. The longest deformation vectors are below a size of 1 mm.

Table 2
Improvement of anatomical overlap, comparing the normalization to the SUIT template with the normalization to the MNI-whole brain template

	Whole-brain Affine	SUIT	Whole-brain Nonlinear	SUIT*
Anatomical correlations				
Atlas sample	0.84	0.97	0.87	0.97
(N=20)	(0.72–0.91)	(0.96–0.97)	(0.81–0.91)	(0.96–0.97)
Cross validation	0.79	0.96	0.86	0.96
(N=16)	(0.63–0.88)	(0.95–0.97)	(0.80–0.90)	(0.95–0.97)
Average fissure distance (mm)				
Cross-validation sample				
Primary fissure	3.96	1.34	3.56	1.41
(Vermal)	(2.23)	(0.40)	(1.93)	(0.37)
Primary fissure	3.97	2.45	3.53	2.43
(Hemisphere)	(1.88)	(1.47)	(1.78)	(1.14)
Intrabiventer	4.14	1.26	2.87	1.23
fissure	(2.05)	(0.29)	(1.11)	(0.26)

Correlations between normalized T1 images were calculated for each possible pairing of individuals. The mean and the interval spanning 95% of the correlations (assuming a normal distribution) were calculated on Fisher-z transformed values, which were subsequently inversely transformed into correlations. The average fissure distance (SD between pairs) is the average distance of two surfaces defining the same fissure, calculated for each possible pair of individuals.

Alignment of fissures

To evaluate the anatomical overlap of cerebellar structures more precisely, we outlined the primary fissure and intrabiventer fissure on the individual anatomies. Both fissures were substantially better aligned using the cerebellar template than when using the whole-brain template (Fig. 7). As a metric of overlap we computed the average distances between corresponding fissures for all possible pairs of participants (Table 2). For the intrabiventer fissure and the vermal portion of the primary fissure, the average inter-fissure distance decreased from 3–4 mm for the two whole-brain normalization methods to 1.3 mm for the SUIT templates. For the hemispheric portion of the primary fissure, the drop in inter-fissure distance was smaller. This reflects the fact that the primary fissure is not as apparent in the hemisphere as in the vermis (Schmahmann et al., 2000), and, as a result, is not visible clearly in the new atlas template. Despite this limitation, the average inter-fissure distance still dropped by 30% compared to the whole-brain normalization.

We also compared alignment of the fissures following an affine instead of nonlinear alignment to the new template. The average inter-fissure distance was 2.5 mm for the vermal portion of the primary fissure and the intrabiventer fissure, double the error achieved with a nonlinear deformation. This underlines the limitations of any procedure that is based on affine transformations only (Grodd et al., 2001).

Overlap of deep cerebellar nuclei

Would the better anatomical overlap obtained with the new method lead to a measurable improvement in the overlap of the deep cerebellar nuclei? This is not a trivial question, as these nuclei are only visible on a T2-weighted image, and not the T1-weighted image that drove our normalization.

Recently, Dimitorva et al. (2005) published a probabilistic atlas of the dentate nuclei. These authors marked the cerebellar nuclei on individual T2-weighted images, and then used nonlinear normalization to the ICBM152 template, implemented in SPM (Ashburner and Friston, 1999). The maximal overlap, i.e., the maximal proportion of individual maps that were marked as deep cerebellar nuclei for the same voxel, was 70%.

We repeated this analysis for the deep cerebellar nuclei of the 16 cross-validation subjects. To be able to compare across studies, we used the same nonlinear normalization method and compared it to the normalization to the SUIT* template. However, similar results were obtained when comparing the affine registration to the ICBM152 with the normalization to the SUIT template.

The bilateral ROI (see Methods) had an average volume of 0.93 cm^3. After nonlinear alignment to the ICBM152 whole-brain template, the individual ROIs were spread out over an area of 4.93 cm^3 with a maximal overlap of 87%. The higher value of the overlap in comparison to past work (Dimitrova et al., 2005) may have resulted from a slightly more generous criterion for including voxels into the ROIs. Using the SUIT* template, the ROIs were distributed over an area of 3.5 cm^3 with a maximal overlap of 100%. The area in which more than 60% of the ROIs overlapped increased from 0.18 cm^3 for the whole-brain ICBM template to 0.42 cm^3 using the SUIT* template. Thus, the new method considerable improved the alignment of fissures in the cerebellar cortex, and also increased the overlap of the deep cerebellar nuclei.

Functional analysis

Finally, we asked whether the improved anatomical overlap would also improve the alignment of the functional data. Again, this is not a trivial question, as it is possible that the inter-individual functional variability is so large that the clear improvements seen in the anatomical alignment would be inconsequential for the analysis of functional data. Possible improvements, however, may be caused by two factors. First, better normalization may improve coverage of cerebellar structures, i.e., an increase in the area for which sufficient data is observed across individuals. Second, better anatomical inter-subject alignment should cause better superposition of the functional areas that are covered, thereby increasing the significance of true activations.

Coverage

Group statistics are typically not calculated on voxels for which data from a certain percentage of participants are missing. If inter-subject alignment is poor, more voxels on the fringe of the cerebellum will “drop out” as not all the edges are precisely aligned to each other. In the first-level GLM we included only voxels with a mean brightness in the EPI images that exceeded a threshold defined by 1/8 of the mean brightness of within-brain voxels. For all other voxels no statistics was calculated and the corresponding voxel in the individual mask image was set to 0. We normalized these mask images into a space defined by the ICBM152 or by SUIT* template, applying the nonlinear deformation that was found between the individual anatomical images and the templates. Because resampling involves trilinear interpolation of voxels in the original image, the normalized mask had continuous values ranging from 0 and 1, indicating the proportion of data observed for that voxel. The mean of these images determines the proportion of data coverage across the group. We

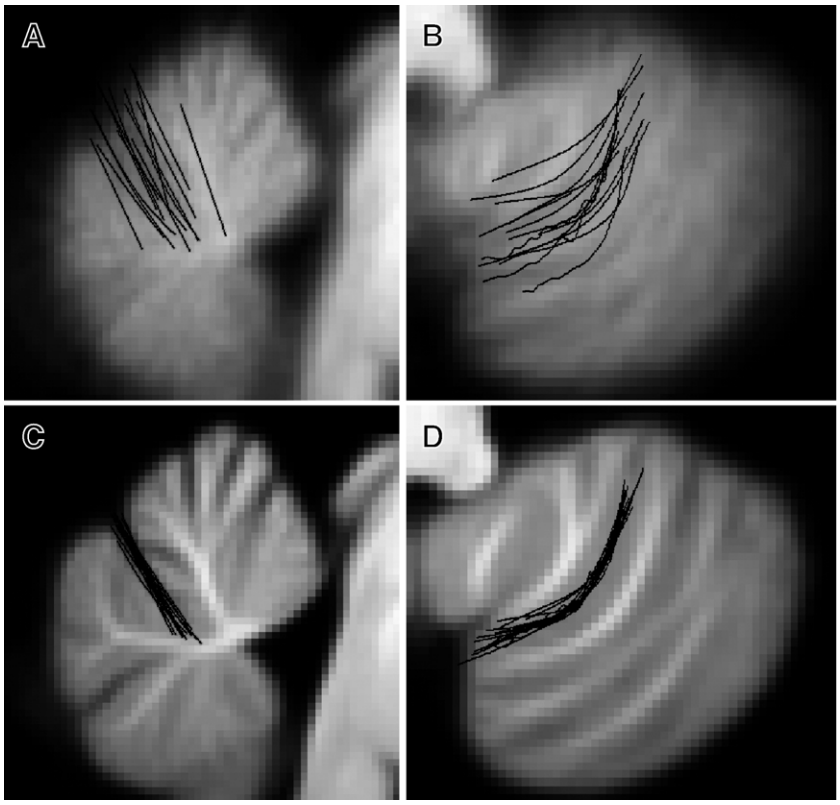

Fig. 7. Location of primary fissure (1st column) and intrabiventer fissure (2nd column) after affine whole-brain normalization (1st row) or after normalization to the cerebellar atlas (2nd row). Fissures were drawn as surfaces using individual anatomies and then normalized. Shown is a slice through the group of normalized fissures, parasagittal ($x=+3$) for the primary fissure, horizontal slice ($z=-55$) for the intrabiventer fissure.

applied a threshold of 80% for data analysis. Using this criterion, the ICBM152 normalization led to coverage of 68% of the anatomically defined cerebellum (excluding brainstem) in Exp 1, and 74% in Exp 2. Part of this is caused by signal dropout and geometrical distortions that occur in the cerebellum due to susceptibility artifacts. Although the new normalization method can not remove these basic limitations in data acquisition, application of the new method reduced the noncovered area by 4.8% for Exp 1 and 5.4% for Exp 2.

Improvements in activation statistics

More important than these relatively modest improvements in coverage was the better superposition of the functional areas. There are at least two movement-related areas in the human cerebellum, one in the anterior cerebellum in lobulus V (extending into VI), and one in the inferior cerebellum in lobules VIIb–VIII (Grodd et al., 2001). If the new normalization method improves functional overlap, the maps of the group statistic for movement against rest contrasts should reflect this both in both the height of the peak values, and in the size of the peaks.

To measure the influence on peak t values, we defined the 5% most activated voxels by averaging the t values based on the ICBM152 and the SUIT* normalized functional data. This ensured that the selection of areas of peak activation was not biased toward one of the templates. Within these areas, we measured the change in t value for the movement vs. rest contrasts when moving from the whole-brain normalization to the SUIT* normalization. The average t values increased by 5–13% depending on contrast and experiment (Fig. 8, Table 3). Improvements were more apparent in Exp 1, but were also clearly noticeable for Exp 2.

We also measured the total cerebellar volume that showed task-related BOLD-signal at an uncorrected statistical threshold of $p<0.001$, a typical value for imaging studies. This volume increased between 5 and 15%, depending on Experiment and contrast (Table 3). The increase in activated volume was calculated only within the area of the cerebellum that was covered by both normalization methods. If one also counts the activated volume in the newly covered areas, then the new method led to 8.3% rather than 6.6% increase in activated volume for Exp 2. This increase is especially apparent in the activated regions on the inferior border of the cerebellum.

Discussion

We present here a cerebellar atlas template that is based on the average geometry of a group of individuals, and at the same time preserves the detail of cerebellar anatomy. The atlas template was created such that it is spatially unbiased, i.e., the location of structures in the template represents the expected location of the corresponding structures in the individual anatomies after affine normalization to the ICBM152 template. Thus, average coordinates within the new SUIT template can be treated as being equivalent to average MNI coordinates, albeit with less spatial variance across individuals. Although 20 participants constitute an admittedly small sample, we show that there are no significant deformation when cross-validating the results with an independent sample of 16 participants.

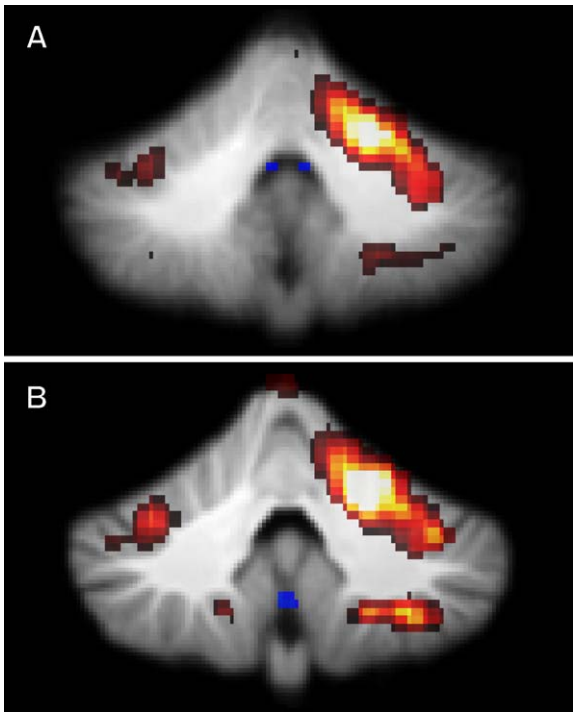

Fig. 8. Functional contrast of arm movements (visual rotation condition) vs. rest from Exp 1 (Diedrichsen et al., 2005), thresholded at $t(12)>5$, $p<0.0002$, uncorrected. After normalization to the SUIT* template (B), peak t values and area of activation increased by 10–14% relative to the standard SPM2 nonlinear alignment to the whole-brain template (A).

The advantage of a voxel-based approach over previous landmark-based approaches (Grodd et al., 2001) is that the new approach is independent of a possibly subjective placing of landmarks and that it allows for nonlinear deformations. Compared to voxel-based whole-brain templates, the new template preserves anatomical information to a higher degree, allowing for improved accuracy of inter-subject alignment for fMRI and lesion studies. We found considerable improvements in the overlap of individual fissures of the cerebellum and of the deep cerebellar nuclei. We also found that these changes lead to more a powerful functional analysis, with improvements in functional activation due to better overlap of about 10–14% in Exp 1, and about 6% in Exp 2. One possible explanation for this difference might be that the participants in Exp 1 were part of the sample used to define the atlas, whereas those in Exp 2 were not. However, we believe this hypothesis unlikely. We showed that the difference in average geometry between the two groups was quite small. Thus, if we had defined the atlas template on the 16 participants in Exp 2, we would have obtained a similar template and consequently a similar functional analysis. Rather, we suspect that the difference between experiments may reflect differences in the degree to which anatomical variability in cerebellar shape contributed to misalignment of the functional data using standard methods.

If a high-resolution template improves the alignment of infratentorial structures, why has this approach not been utilized for the cerebral cortex? The answer lies, we believe, in the large inter-individual variability of cortical folding patterns, which increases as one moves away from primary sensory and motor regions (Van Essen, 2005). Thus, an average template that approximates the outline of the cerebral cortex is likely the best that can be achieved using 3d-normalization. Considerable improvements in inter-individual alignment for the cortex can be obtained by flattening the cortical sheet and using 2d-normalization techniques (Fischl et al., 1999; Van Essen, 2005). The lobular structure of the cerebellum, in contrast, is quite stable across individuals, allowing for accurate alignment of individual lobules in three dimensions.

Using the new technique requires two steps. In the first step the cerebellum and brainstem are isolated from the surrounding tissue. We developed a Bayesian algorithm to perform this task. However, the algorithm is not completely fail-proof and small hand corrections are necessary in many cases. Given that these can be performed in a relatively short time (5–10 min per individual), we feel that the additional effort is quite justified. The second step is fully automated and leads to nonlinear normalization of the isolated cerebellum and brainstem to the new atlas template. The resulting deformation can then be applied to functional or lesion data for that individual.

The new atlas has some important limitations. First, it should be noted that the template was defined on young, neurological healthy individuals ranging in age from 22 to 45 years. For research concerning the cerebellar anatomy in children, adolescents or senior individuals, a specialized atlas template should be created. The nonlinear atlas generation algorithm proposed here offers a simple and efficient way to perform this task.

The second limitation is inherent in normalization using cosine basis functions. While computationally very efficient, we found that the resulting deformations sometimes showed rippling artifacts, as are visible in Fig. 6. Because these deformations are below 1 mm, they would not change functional analysis or lesion overlap analysis to any appreciable degree. However, if deformation maps are used to compute local expansions and compressions to evaluate possible neuroanatomical changes in pathological populations, these artifacts may play a role. For the study of small-scale anatomical differences, we are currently working to employ alternative algorithms that do not use basis functions (Joshi and Miller, 2000). These changes should avoid the rippling artifact observed here and will result, we hope, in deformation maps that can be used for fine-grained morphometric analysis. However, for the analysis of standard resolution functional imaging and lesion data, we believe that the cosine basis function approach is sufficient, and may be preferable to other algorithms given its computational efficiency and broad popularity.

The atlas templates and the code for segmentation and normalization, implemented in MATLAB® and SPM2, can be downloaded freely from http://www.bangor.ac.uk/~pss412/imaging/suit.htm. Along with the atlas we provide a flat representation of the colin27 cerebellum (Van Essen, 2002a) in

Table 3
Percent improvement in the functional group analysis, comparing the normalization to the SUIT* template with the nonlinear normalization to the ICBM152 whole-brain template

	Exp 1 ($N=12$)		Exp 2 ($N=16$)	
T value for highest 5%	11.20%	(10.2–12.7)	6.10%	(4.8–6.8)
Volume with $p<0.001$	12.20%	(10.5–14.3)	6.60%	(4.9–8.0)

For cerebellar voxels only, we calculated the change in t value for the 5% most activated voxels and the change in the suprathreshold volume ($p<0.001$, uncorrected). The values were calculated for 3 basic contrasts for Experiment 1 and Experiment 2 from Diedrichsen et al. (2005). Mean values and the range across contrasts are shown.

the reference frame of the new template, such that functional data can be visualized in 2D. We also provide MATLAB code that translates coordinates between the new atlas space and the space defined by the colin27 cerebellum. Although the colin27 atlas cerebellum was aligned to the MNI space, it would be inaccurate to use MNI coordinates to reference the corresponding location in the annotated atlas of the colin27 brain (Schmahmann et al., 2000). As any other individual, the colin27 cerebellum shows deformations up to a size of 9 mm relative to the expected location of structures in MNI space. By using the provided nonlinear translation functions, locations of structures in the colin27 cerebellum (Schmahmann et al., 2000) can now be more accurately related to their average MNI coordinates across the population.

In summary, we present here a time-efficient, voxel-based method to improve the alignment of infra-tentorial anatomical and functional areas. While our evaluation has focused on the cerebellum, similar improvements are likely to be present for brainstem structures as well. We therefore believe that the method presented here constitutes a valuable addition to the toolkit of the neuroscientist with an interest in the anatomy and function of the cerebellum and brainstem.

Acknowledgments

This work was supported through grants from the NIH (NS37422), the Human Frontiers Science Program, and the Johns Hopkins General Clinical Research Center (RPN 02-08-15-03). I am grateful to the staff of the F.M. Kirby Research Center for Functional Brain Imaging at Kennedy Krieger Institute, funded by an NIH/NCRR resource grant (RR15241), and to Scott Grafton, Reza Shadmehr, and Sarah Ying for the helpful comments and support.

References

Albus, J.S., 1971. A theory of cerebellar function. Math. Biosci. 10, 25–61.

Ashburner, J., Friston, K.J., 1999. Nonlinear spatial normalization using basis functions. Hum. Brain Mapp. 7, 254–266.

Ashburner, J., Friston, K.J., 2005. Unified segmentation. NeuroImage 26, 839–851.

Ashburner, J., Neelin, P., Collins, D.L., Evans, A., Friston, K., 1997. Incorporating prior knowledge into image registration. NeuroImage 6, 344–352.

Courchesne, E., Allen, G., 1997. Prediction and preparation, fundamental functions of the cerebellum. Learn. Mem. 4, 1–35.

Desmond, J.E., Gabrieli, J.D., Wagner, A.D., Ginier, B.L., Glover, G. H., 1997. Lobular patterns of cerebellar activation in verbal working-memory and finger-tapping tasks as revealed by functional MRI. J. Neurosci. 17, 9675–9685.

Desmond, J.E., Gabrieli, J.D., Glover, G.H., 1998. Dissociation of frontal and cerebellar activity in a cognitive task: evidence for a distinction between selection and search. NeuroImage 7, 368–376.

Diedrichsen, J., Shadmehr, R., 2005. Detecting and adjusting for artifacts in fMRI time series data. NeuroImage 27, 624–634.

Diedrichsen, J., Hashambhoy, Y.L., Rane, T., Shadmehr, R., 2005. Neural correlates of reach errors. J. Neurosci. 25, 9919–9931.

Dimitrova, A., Zeljko, D., Schwarze, F., Maschke, M., Gerwig, M., Frings, M., Beck, A., Aurich, V., Forsting, M., Timmann, D., 2005. Probabilistic 3D MRI atlas of the human cerebellar dentate/interposed nuclei. NeuroImage.

Evans, A.C., Collins, D.L., Mills, S.R., Brown, E.D., Kelly, R.L., Peters, T.M., 1993. 3D statistical neuroanatomical models from 305 MRI volumes. Proc. IEEE-Nucl. Sci. Symp. Med. Imaging Conf. 1813–1817.

Fischl, B., Sereno, M.I., Tootell, R.B., Dale, A.M., 1999. High-resolution intersubject averaging and a coordinate system for the cortical surface. Hum. Brain Mapp. 8, 272–284.

Friston, K., Holmes, A.P., Ashburner, J., 1999. Statistical Parameter mapping (SPM). Available on line at http://www.fil.ion.ucl.ac.uk/spm/.

Gao, J.H., Parsons, L.M., Bower, J.M., Xiong, J, Li, J., Fox, P.T., 1996. Cerebellum implicated in sensory acquisition and discrimination rather than motor control. Science 272, 545–547.

Grodd, W., Hulsmann, E., Lotze, M., Wildgruber, D., Erb, M., 2001. Sensorimotor mapping of the human cerebellum: fMRI evidence of somatotopic organization. Hum. Brain Mapp. 13, 55–73.

Ivry, R.B., Spencer, R.M., Zelaznik, H.N., Diedrichsen, J., 2002. The cerebellum and event timing. Ann. N. Y. Acad. Sci. 978, 302–317.

Joshi, S.C., Miller, M.I., 2000. Landmark matching via large deformation diffeomorphisms. IEEE Trans. Image process. 9, 1357–1370.

Kelly, R.M., Strick, P.L., 2003. Cerebellar loops with motor cortex and prefrontal cortex of a nonhuman primate. J. Neurosci. 23, 8432–8444.

Makris, N., Hodge, S.M., Haselgrove, C., Kennedy, D.N., Dale, A., Fischl, B., Rosen, B.R., Harris, G., Caviness Jr., V.S., Schmahmann, J.D., 2003. Human cerebellum: surface-assisted cortical parcellation and volumetry with magnetic resonance imaging. J. Cogn. Neuro. 15, 584–599.

Makris, N., Schlerf, J.E., Hodge, S.M., Haselgrove, C., Albaugh, M.D., Seidman, L.J., Rauch, S.L., Harris, G., Biederman, J., Caviness Jr., V.S., Kennedy, D.N., Schmahmann, J.D., 2005. MRI-based surface-assisted parcellation of human cerebellar cortex: an anatomically specified method with estimate of reliability. NeuroImage 25, 1146–1160.

Middleton, F.A., Strick, P.L., 1997. Cerebellar Output Channels. In: Schahmann, J.D. (Ed.), The Cerebellum and Cognition. Academic Press, San Diego, CA, pp. 31–60.

Pierson, R., Corson, P.W., Sears, L.L., Alicata, D., Magnotta, V., Oleary, D., Andreasen, N.C., 2002. Manual and semiautomated measurement of cerebellar subregions on MR images. NeuroImage 17, 61–76.

Pruessmann, K.P., Weiger, M., Scheidegger, M.B., Boesiger, P., 1999. SENSE: sensitivity encoding for fast MRI. Magn. Reson. Med. 42, 952–962.

Schmahmann, J.D., 1996. From movement to thought: anatomic substrates of the cerebellar contribution to cognitive processing. Hum. Brain Mapp. 4, 174–198.

Schmahmann, J.D., Doyon, J., Toga, A., Petrides, M., Evans, A., 2000. MRI Atlas of the Human Cerebellum. Academic Press, San Diego.

Talairach, J., Tournoux, P., 1988. Co-planar Stereotaxic Atlas of the Human Brain: 3-Dimensional Proportional System: An Approach to Cerebral Imaging. Thieme, New York.

Thach, W.T., Goodkin, H.P., Keating, J.G., 1992. The cerebellum and the adaptive coordination of movement. Annu. Rev. Neurosci. 15, 403–442.

Van Essen, D.C., 2002a. Surface-based atlases of cerebellar cortex in the human, macaque, and mouse. Ann. N. Y. Acad. Sci. 978, 468–479.

Van Essen, D.C., 2002b. Windows on the brain: the emerging role of atlases and databases in neuroscience. Curr. Opin. Neurobiol. 12, 574–579.

Van Essen, D.C., 2005. A population-average, landmark- and surface-based (PALS) atlas of human cerebral cortex. NeuroImage 28, 635–662.

Van Essen, D.C., Dickson, J., Harwell, J., Hanlon, D., Anderson, C.H., Drury, H.A., 2001. An integrated software system for surface-based analyses of cerebral cortex. J. Am. Med. Inf. Assoc. 41, 1359–1378.

Wolpert, D.M., Miall, R.C., Kawato, M., 1998. Internal models in the cerebellum. Trends Cogn. Sci. 2, 313–321.

Woods, R.P., Grafton, S.T., Watson, J.D., Sicotte, N.L., Mazziotta, J.C., 1998a. Automated image registration: II. Intersubject validation of linear and nonlinear models. J. Comput. Assist. Tomogr. 22, 153–165.

Woods, R.P., Grafton, S.T., Holmes, C.J., Cherry, S.R., Mazziotta, J.C., 1998b. Automated image registration: I. General methods and intrasubject, intramodality validation. J. Comput. Assist. Tomogr. 22, 139–152.

Worsley, K.J., Marrett, S., Neelin, P., Vandal, A.C., Friston, K.J., Evans, A.C., 1996. A unified statistical approach for determining significant voxels in images of cerebral activation. Hum. Brain Mapp. 12, 900–918.